Soil Biology and Biochemistry 129 (2019) 1–12

Contents lists available at ScienceDirect

Soil Biology and Biochemistry

journal homepage: www.elsevier.com/locate/soilbio

Predicting the decomposability of arctic tundra soil organic matter with mid infrared spectroscopy

Roser Matamala[a,*], Julie D. Jastrow[a], Francisco J. Calderón[b], Chao Liang[a,2], Zhaosheng Fan[a,1], Gary J. Michaelson[c], Chien-Lu Ping[c]

[a] Environmental Science Division, Argonne National Laboratory, Argonne, IL, 60439, USA
[b] USDA-ARS, Central Plains Research Station, Akron, CO, 80720, USA
[c] School of Natural Resources and Extension, University of Alaska Fairbanks, Palmer, AK, 99645, USA

ARTICLE INFO

Keywords:
MIR spectroscopy
Tundra soil incubations
Mineralization of SOM
PLSR predictive models

ABSTRACT

Vast amounts of soil organic matter (SOM) have been preserved in arctic soils over millennia time scales due to the limiting effects of cold and wet environments on decomposer activity. With the increase in high latitude warming due to climate change, the potential decomposability of this SOM needs to be assessed. In this study, we investigated the capability of mid infrared (MIR) spectroscopy to quickly predict soil carbon and nitrogen concentrations and carbon (C) mineralized during short-term incubations of tundra soils. Active layer and upper permafrost soils collected from four tundra sites on the North Slope of Alaska were incubated at 1, 4, 8 and 16 °C for 60 days. All incubated soils were scanned to obtain the MIR spectra and analyzed for total organic carbon (TOC) and total nitrogen (TN) concentrations, and salt-extractable organic matter carbon (SEOM). Partial least square regression (PLSR) models, constructed using the MIR spectral data for all soils, were excellent predictors of soil TOC and TN concentrations and good predictors of mineralized C for these tundra soils. We explored whether we could improve the prediction of mineralized C by splitting the soils into the groups defined by the influential factors and thresholds identified in a principal components analysis: (1) TOC > 10%, (2) TOC < 10%, (3) TN < 0.6%, (4) TN > 0.6%, (5) acidic tundra, and (6) non-acidic tundra. The best PLSR mineralization models were found for soils with TOC < 10% and TN < 0.6%. Analysis of the PLSR loadings and beta coefficients from these models indicated a small number of influential spectral bands. These bands were associated with clay content, phenolics, aliphatics, silicates, carboxylic acids, and amides. Our results suggest that MIR could serve as a useful tool for quickly and reasonably estimating the initial decomposability of tundra soils, particularly for mineral soils and the mixed organic-mineral horizons of cryoturbated soils.

1. Introduction

Improving projections of future carbon (C) release from warming permafrost-region soils requires more information on the potential decomposability of organic matter stored in these soils (Schädel et al., 2014: Schuur et al., 2015). Although incubation studies depart from field conditions, they are useful for assessing and comparing the potential decomposability of organic matter by measuring the amount of C that can be mineralized in different soils and for parsing out the effects of various controlling factors that are difficult to separate under field conditions. Soil incubations have been used extensively to evaluate the mineralization of soil organic matter (SOM) stored in these soils (e.g., Nadelhoffer et al., 1991; Neff and Hooper, 2002; Weintraub and Schimel, 2003; Fierer et al., 2006; Shaver et al., 2006; Uhlířová et al., 2007; Lee et al., 2012; Elberling et al., 2013; Knoblauch et al., 2013; Wild et al., 2014; Yang et al., 2016). The potential decomposability of Arctic soils has been shown to increase with rising temperature because a substantial amount of the SOM is easily converted into carbon dioxide (CO_2) under favorable conditions (Neff and Hooper, 2002; Weintraub and Schimel, 2003; Dutta et al., 2006; Waldrop et al., 2010; Lee et al., 2012; Knoblauch et al., 2013).

Because potential decomposability of SOM in soils is usually determined by doing soil incubations, which are a substantial investment of both time and space, a number of studies have examined the ability

* Corresponding author. Environmental Science Division, Building 203, E-145, Argonne National Laboratory, Argonne, IL, 60439, USA.
E-mail address: matamala@anl.gov (R. Matamala).
[1] Present address: USDA–ARS Research Unit, the Jornada, Las Cruces, NM, 88003, USA.
[2] Present Address: Institute of Applied Ecology, Chinese Academy of Sciences, Shenyang, 110016, China.

https://doi.org/10.1016/j.soilbio.2018.10.014
Received 9 July 2018; Received in revised form 13 October 2018; Accepted 22 October 2018
Available online 25 October 2018
0038-0717/

of various indicators/proxies to predict litter and SOM decomposition (e.g., Bruun et al., 2005; Leinweber et al., 2008; Thomsen et al., 2009; Mann et al., 2015; Soong et al., 2015). In assessing plant litter decomposability, Bruun et al. (2005) found that near infrared reflectance spectra were a much better predictor of C mineralization than litter carbon:nitrogen (C:N) ratios and marginally better than the more time-consuming chemical digestion methods often used to characterize litter quality. In soil incubation studies, CO_2 production (on a mass basis) is generally well correlated with total SOM (Neff and Hooper, 2002; Dutta et al., 2006; Knoblauch et al., 2013), but soil differences in decomposability are better assessed by comparing CO_2 production normalized to soil C. Although some studies have suggested that soil C:N ratio could be a good predictor of the decomposability of SOM pools with decadal turnover times (Schädel et al., 2014), other, more sophisticated predictors based on the molecular composition of SOM are also being explored (Thomsen et al., 2009; Gillespie et al., 2014; Mann et al., 2015). Thomsen et al. (2009) calibrated near infrared reflectance spectra of bulk soil to reasonably predict CO_2 produced during 238-day incubations of 37 agricultural soils. Both mineralized C and N could be predicted with moderate accuracy using this technique (Soriano-Disla et al., 2014). Using the same soils obtained by Thomsen et al. (2009), Peltre et al. (2014), produced fair predictive models for the 238-day incubations by using Fourier transform mid-infrared photoacoustic spectroscopy. Gillespie et al. (2014) used X-ray absorption near-edge structure spectroscopy to determine the SOM composition of cryoturbated subarctic soils and found that ratios of carbohydrate:ketone and carboxylic acid:ketone were good predictors of mineralized C in 98-day incubation bioassays. Mann et al. (2015) proposed an index of potential decomposability that is based on codifying the molecular C, hydrogen (H), and oxygen (O) contents of SOM components according to their observed degradation potentials in soil incubation studies. This CHO index was developed using Fourier-transform ion cyclotron resonance mass spectrometry to detect the relative H, O, and C content in organic molecules. Clearly, spectroscopy methods appear to be most useful and they are being widely used in the search for SOM mineralization proxies.

We have determined that diffuse reflectance infrared Fourier transform (DRIFT) spectra contain valuable information about SOM chemical composition and environmental site conditions for northern cold-region soils (Matamala et al., 2017). In that study, DRIFT spectra were very sensitive to the degradation state of SOM, as shown by spectral differences among organic horizons (Oa, Oe, Oi) defined by the decomposition stage of the organic matter (Oi, high fiber content, > 75%, and representing the lowest degree of decomposition; Oa, low fiber content, < 17%, and representing the highest degree of decomposition, and Oe, moderate decomposition degree with fiber content between 17 and 75%). This was suggested by greater absorbance of −O−H//N−H and aliphatic bonds and carbohydrates, which are indicative of lower decomposition, in the Oi horizons compared to the Oa horizons, which contained greater aromatics, carboxylates and carboxylic structures (Matamala et al., 2017). In addition, the spectra were related to many soil/site attributes including soil C and N contents, parent material, land cover type, permafrost presence and other factors directly related to those attributes, such as, soil drainage, soil depth, bulk density, cation exchange capacity, and pH, which can affect the decomposability of organic matter in soils. Considering that much of the organic matter preserved in permafrost region soils is peat-like, or highly enriched in lightly decomposed particular organic matter, it is reasonable to assume that decomposability of SOM in tundra soils might be examined by using mid infrared spectroscopy (MIR) because it strongly absorbs in regions attributable to labile C organic functional groups (Tinti et al., 2015; Calderón et al., 2017).

Our goal in this study was to determine whether MIR characterization of the bulk organomineral composition of tundra soils can be used to predict their potential decomposability, as indicated by short-term C mineralization during laboratory incubations. We hypothesized that beyond the known capability of MIR spectra to predict the total organic C (TOC) and total nitrogen (TN) of many soils (Soriano-Disla et al., 2014), the ability of MIR to discriminate variations in both specific organic functional groups (particularly those associated with readily decomposable organic compounds), and soil minerals, will enable the development of calibration models suitable for predicting the short-term mineralization of SOM in tundra soils. Exploration of these models should also help identify soil components (e.g., SOM functional groups, mineral properties) that are influential in predicting initial SOM decomposability and inform future studies investigating the interactions of soil properties and environmental/site factors in determining the fate of C stocks stored in tundra soils in a changing climate.

2. Materials and methods

2.1. Study sites and soil sampling

Soil samples were collected from four tundra sites located on the Arctic Coastal Plain (near Prudhoe Bay) and the Arctic Foothills (Sagwon Hills and Happy Valley) of Alaska (Table 1). Three of the sites supported acidic tundra. Common plant species at these sites included *Betula nana, Carex bigelowii, Cassiope tetragona, Cetraria cucullata, Cladonia stygia*, *Dactylina arctica, Eriophorum vaginatum, Ledum decumbens, Polygonum viviparum, Vaccinium vitis-idaea, Vaccinium uliginosum, Racomitrium lanuginosum,* and *Sphagnum sp*. Vegetation at the fourth site was non-acidic tundra and differed from the acidic tundra sites. Dominant species included *Tomentypnum nitens*, *Arctostaphylos rubra*, *Carex aquatilis, Dryas integrifolia, Eriophorum angustifolium, Salix arctica, and Salix reticulata* (Michaelson and Ping, 2017). Two of the sites were located in lowland areas with very poorly drained soils that formed on alluvium parent material. The other two sites were positioned in upland areas with poorly drained soils formed on loess and loess/moraine parent materials (Table 1).

Soils were sampled by opening a pit (approximately 1 m^3) using shovels and a jack hammer. The depth of the active layer was determined by identifying changes in soil/ice cryostructures within the soil profile (Ping et al., 2013). Active layer samples representing both the surface organic horizon and the underlying mineral horizon (about 12 L each) were obtained by cutting large blocks from the exposed pit face. Frozen bulk samples of similar size were obtained from the upper permafrost by using the jack hammer. At all sites, the upper permafrost was composed of a cryoturbated horizon with intermixed organic and

Table 1
Study site locations and selected characteristics.

Physiography/name	Latitude/Longitude	Land cover[a]	Microtopography	Parent material[b]	Drainage class[b]	Soil type[c]
Coastal Plain lowland (CL)	69.989450 N −148.68642 W	WNT	low-centered polygons	alluvium	very poor	Ruptic-Histic Aquiturbel
Sagwon Hills lowland (SL)	69.383517 N −148.74088 W	MAT	high-centered polygons	alluvium	very poor	Glacic Histoturbel
Sagwon Hills upland (SU)	69.425283 N −148.69512 W	MAT	non-sorted circles	loess	poor	Ruptic-Histic Aquiturbel
Happy Valley upland (HU)	69.148467 N −148.84565 W	MAT	non-sorted circles	loess/moraine	poor	Ruptic Histoturbel

[a] Landcover type: moist acidic tundra, MAT; wet non-acidic tundra, WNT; Walker et al. (2004).
[b] Michaelson and Ping (2017).
[c] Michaelson et al. (2013).

mineral components. Samples were kept in a cooler in the field and then stored in a freezer before shipping to the laboratory, where they were kept in a freezer room at −20 °C until incubations commenced.

2.2. Decomposability of tundra soils

In the freezer room, the entire bulk sample from each horizon at each site was chopped into pieces (about 4- to 9-cm^3) with a hammer and chisel and then thoroughly mixed. To ensure a similar volume of soil in each incubation unit, variable combinations of frozen soil pieces were randomly selected to fill a plastic cylinder that was placed inside a 250-ml glass jar. The bottom of each cylinder contained a metal mesh covered with a glass fiber filter (Whatman GF/A) to support the soil. Each cylinder was placed on a tubular plastic base that lifted the cylinder off the floor of the jar by 3 cm and allowed excess water to drain by gravity upon thawing. This method of thawing and drainage maintained the overall structure of soils with high ice contents by preventing the collapse that would have happened during rapid thaw without drainage. The jar lids were equipped with quick connect fittings that allowed for air sampling.

Soils were incubated at four temperatures, 1, 4, 8, and 16 °C, by placing jars in a circulating ethylene glycol bath that maintained soil temperatures at ± 0.2 °C of the target. The ethylene glycol bath was set inside a chest freezer, and the target temperature was achieved by balancing the cooling from the freezer with heating by an immersion circulator inside the bath. The incubation system was similar to that used by Michaelson and Ping (2003) and Schimel and Mikan (2005). A total of 240 soil samples (4 temperatures × 4 sites × 3 horizons × 5 replicates) were incubated for 60 days. CO_2 production rates were measured with an automated closed-system respirometer equipped with a CO_2 non-dispersive infrared detector (Micro-Oxymax, Columbus Instruments). Respiration rates in each jar (automatically corrected for headspace volume and time) were measured about four times per day periodically throughout the duration of the incubation.

The measured CO_2 production rate (μL CO_2 g dry $soil^{-1}$ hr^{-1}) for each sample was fitted to a two-pool exponential decay model, CO_2 production rate = a * exp (-b * hours) + c * exp (-d * hours).

Where a, b, c, and d parameters were estimated with the Curve Fit Wizard in SigmaPlot 13.0 (Systat Software, Inc.). Initial CO_2 measurements, up to the first 24 h, were removed before fitting the model to avoid inclusion of soil thawing effects. The total C mineralized at the end of the 60-day incubation was determined by integrating the exponential decay curve for each sample, after adjusting for incubation temperature and pressure using the ideal gas law. To determine whether the capability of MIR to predict short-term C mineralization was affected by incubation length, we also integrated the decay curve to determine the amount of C mineralized after 7, 15 and 30 days of incubation.

2.3. Soil analysis

At the end of the 60-day incubation period, all incubated soils were frozen at −20 °C and then lyophilized. The soils were then sieved (< 2-mm), pulverized for 2 min in a stainless-steel high energy ball mill (8000D Mixer/Mill; Spex SamplePrep, Metuchen, New Jersey), oven dried overnight at 65 °C, and analyzed by dry combustion with an elemental analyzer (vario Max cube; Elementar Americas, Ronkonkoma, New York) at 650 °C for TOC and at 900 °C for total carbon (TC) and TN (Provin, 2014).

MIR spectra were generated for all incubated soils by DRIFT spectroscopy using a Spectrum 100 Series spectrometer (PerkinElmer, Waltham, Massachusetts) equipped with a potassium bromide (KBr) beam splitter, a deuterated triglycine sulphate detector, and a 60-cup AutoDiff diffuse-reflectance accessory (Pike Technologies, Madison, Wisconsin). Immediately before analysis, each soil was further homogenized and mixed by hand with an agate mortar and pestle. Five replicate aliquots of each soil sample were carefully loaded into AutoDiff sample cups and leveled with a spatula. The aliquots were scanned against a KBr background. Spectra were obtained in reflectance units and converted to pseudoabsorbance (log [1/Reflectance]) by using PerkinElmer Spectrum 10 software. Each spectra was collected at 1 cm^{-1} resolution over the range of 4000–450 cm^{-1} wavenumbers (wn). An average spectrum per each incubated soil was obtained from the five aliquots after removing any spectral outliers. Spectra were baseline corrected before performing averages or other analysis. Spectral signals from water were observed at 3600-3000 cm^{-1} in all soils because samples were dried at 65 °C to minimize thermal degradation of labile organic constituents and related impacts on TOC concentrations (Duboc et al., 2016; Stumpe et al., 2011).

As a proxy for initial bioavailable SOM, the C concentration of salt-extractable organic matter (SEOM) was determined for non-incubated subsamples of dried, 2-mm sieved soil (method modified from Chantigny et al., 2008) by averaging 13 replicated extractions for each horizon and site combination. A constant volume of soil (4.5 cm^3) was weighed after drying at 65 °C for 2 h and extracted for 1 h with 45 mL of 0.5 M K_2SO_4 in a 50-mL centrifuge tube at low speed on a reciprocating shaker (180 oscillations/min). SEOM extracts were isolated by centrifugation at 1000 × g for 10 min followed by vacuum filtration of supernatants through a 0.45 μm cellulose nitrate filter. Extracts were frozen at −20 °C, and later thawed and thoroughly mixed before analysis with a TOC-V_{CPH} combustion oxidation analyzer (Shimadzu Scientific Instruments, Columbia, Maryland).

2.4. Data analysis

Statistical differences in mineralized C at the end of the 60-day incubation due to site, horizon, and temperature were tested by Three Way ANOVA and Pairwise Multiple Comparison (Holm-Sidak method) analysis with SigmaPlot 13.0 (Systat Software, Inc.). We also examined the relationship between mineralized C with TOC, TN, C:N ratio, and initial SEOM by regression analysis and tested significance of slope and intercept using t-test statistics package with SigmaPlot 13.0. Principal component analysis (PCA) of the MIR spectra was conducted with PC-ORD (MjM Software Design, Gleneden Beach, Oregon) to determine variables (site, tundra type, soil horizon, incubation temperature, soil TOC and TN concentrations, and soil C:N ratios) that most influenced the spectra. Pearson and Kendall correlations between these variables and the first three principal components were used to determine the influential variables. Predictive models for soil TOC, TN, C:N, and mineralized C were developed from the soil MIR spectra by using partial least squares regression (PLSR) with Grams IQ Software version 9.3 (Thermo Fisher Scientific, Waltham, Massachusetts). These predictive models used the whole dataset. For the mineralized C, we split the calibration dataset into the groups identified by the PCA and conducted new PLSR analyses for each of the groups that were correlated, separately, to explore the potential for improving the predictive capability of the mineralized C model. For each predictive model, the analytical measurements were square root transformed to normalize the data and to improve the homogeneity of residuals and reduce non-linearity of the calibration models. Model performance was tested by leave-one-out random cross validation using all 240 soil samples. Spectral preprocessing, such as pathlength correction or derivative calculations, were tested and discarded because they did not substantially affect model performance (R^2 increase < 2%). The spectra were mean centered before PLSR, and outliers were identified and removed by using a Mahalanobis Distance threshold of three. The optimal number of factors for the model were determined by calculating the predicted residual error sum of squares (PRESS), the F ratio (F $ratio_i$ = $PRESS_i/PRESS_{min}$), and the PRESS F-test of each factor to identify the significant number of factors that minimize PRESS ratio (α = 0.25 significance level, F-test P < 0.75) (Duckworth, 1998). The predictive capability of the calibration models was assessed on the basis of the coefficient of

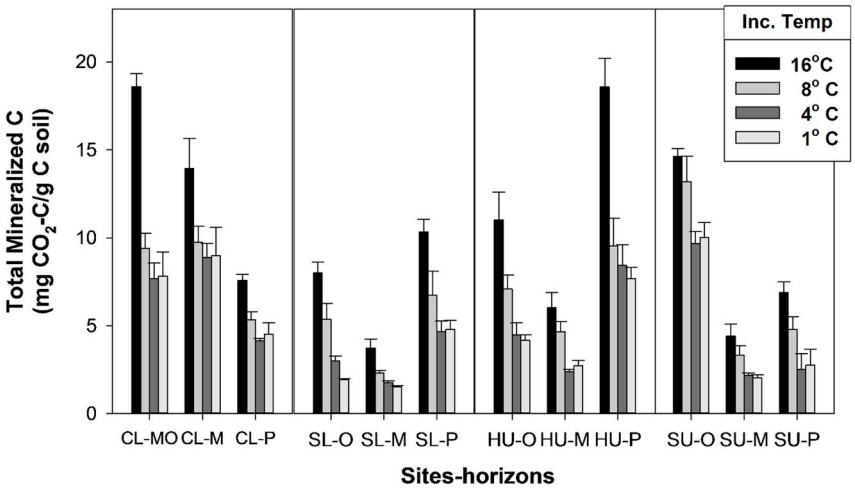

Fig. 1. Total mineralized C at the end of the 60-day incubation of tundra soils at 1, 4, 8, and 16 °C in active layer organic (O), active layer organic-mineral (MO), active layer mineral (M), and mixed organic/mineral upper permafrost (P) horizons at each site.

determination (R^2), the root mean square error of prediction or standard error of prediction (RMSE or SEP, respectively), and the ratio of performance to interquartile distance (RPIQ). RPIQ was calculated as RPIQ = $(Q_3 - Q_1)/SEP$ (Bellon-Maurel et al., 2010). High R^2, low RMSE, and RPIQ values > 2 indicate the best predictive models (Bellon-Maurel et al., 2010). Inferences about the qualitative drivers of correlations between the soil measurements and the MIR spectra were derived from the PLSR loadings and β coefficients.

3. Results

Mineralized C varied by site, horizon, and temperature (Fig. 1). In general, mineralized C appeared to increase with rising temperature for most sites and horizons, but significant differences were only found between 16 °C and the other temperatures ($P = 0.03$), and the amount of C mineralized at 8 °C, 4 °C and 1 °C did not differ significantly across each other (Fig. 1). Mineralized C differed significantly between Coastal Plain and Sagwon Hills lowland sites ($P = 0.007$), and between organic and mineral active layer horizons ($P = 0.006$) across sites. The variations in amount of C mineralized among soils after the 60-day incubations ranged from 18.6 to 1.5 mg CO_2–C/g C soil (Fig. 1) and provided a broad gradient of soil decomposability useful for exploring the development of MIR calibration models (Fig. 2A).

The TOC and TN concentrations of the incubated soils ranged from almost 500 to 13 mg C/g soil and from 29 to 0.7 mg N/g soil, respectively (Fig. 2B and C). The highest TOC and TN concentrations occurred in the active-layer organic and permafrost soils, with Sagwon Hills lowland and Happy Valley organic soils having more than twice the amount of the other soils (Fig. 2B and C). The Coastal Plain site did not have an active-layer organic horizon like the other sites, instead the active-layer organic was low in TOC and it was labeled as an active-layer mineral-organic (MO) horizon. However, as it had a substantial amount of TOC compared to the active-layer mineral that was sampled underneath it was incubated and analyzed separately. The lowest TOC and TN concentrations were found in the active-layer mineral soils (Fig. 2B and C). The Coastal Plain soils were the only ones containing inorganic C (data not shown). Most soil C:N ratios ranged between 21 and 14, but the Sagwon Hills upland site's active-layer organic soil, at 37, was exceptionally high (Fig. 2D). Initial soil SEOM ranged from 15 to 6 mg C/g C soil (Fig. 2E). SEOM in soil was directly related to the amount of mineralized C at the end of the 60-day incubation (Mineralized C = 0.958 * SEOM - 2.43; slope $P = 0.0003$ and an $R^2 = 0.7576$) (Fig. S1 Supplemental Material), while neither TOC, TN or the C:N ratio were related to mineralized C.

The MIR spectra of the incubated soils were not affected by incubation temperature but they were influenced by tundra type (acidic versus non-acidic tundra) and amount of TOC and TN concentrations in the soil (Fig. 3). In the PCA analyses, PC1 explained 75.4% of the variance, PC2 explained 13.3%, and PC3 explained 5.7%. PC1 was strongly correlated ($P < 0.0001$) with TOC and TN content – distinctly separating soils with high TOC and TN concentrations from those with low TOC ($r = -0.90$) and TN ($r = -0.89$) concentrations (Fig. 3). A clear threshold in the PCA for TOC concentrations was observed at about 100 mg C/g soil; most soils with TOC concentrations above this threshold had positive PC1 scores and soils with lower TOC concentrations had negative PC1 scores (Fig. 3 insert). A similar separation along PC1 occurred for TN at about 6 mg N/g soil (data not shown). Although PC2 was not correlated with any of the studied variables, PC3 was correlated with tundra type ($P < 0.01$, $r = 0.69$) separating acidic from non-acidic tundra (Fig. 3). Most acidic tundra soils had negative PC3 scores, whereas non-acidic tundra soils had positive PC3 scores.

For simplicity, and because temperature did not affect the MIR spectra of soils, we averaged the soil spectral data by site (tundra type) and horizon (in lieu of TOC and TN concentrations) in Fig. 4, and the wn peaks identified by the GRAMS software for those spectra are reported in Table 2. Differences in absorbance intensity were found across sites and horizons, with generally greater absorbance intensities for organic soils and lower intensities for mineral soils at most wn (Fig. 4). A total of 25 peaks were identified by the GRAMS software. Four peaks were present at all sites and horizons (Fig. 4; Table 2). Peaks at wn 3394 and 1159 cm^{-1} and at wn 2924 and 2852 cm^{-1} (except for Coastal Plain active-layer mineral-organic and mineral horizons where the peaks were found at 2984 and 2877 respectively) were present in all soils and sites. A peak at wn 811 cm^{-1} was found in the spectra of all soils except Sagwon Hills lowland organic soils. Peaks at wn 3622, 1993, 1870, 1616, and 1000 cm^{-1} occurred in all but the Sagwon Hills lowland organic and Happy Valley organic soils. Peaks at wn 1521 cm^{-1} were found in all soils except Coastal Plain active layer mineral-organic and mineral soils. Peaks at wn 1423 cm^{-1} were found in all soils except in the mineral Sagwon Hills upland and Happy Valley soils, and at 1380 cm^{-1} which were found in all soils except in the permafrost Sagwon Hills lowland and Happy Valley soils. The remaining peaks occurred inconsistently across sites or horizons. For example, a peak at wn 873 cm^{-1} was found in all Coastal Plain and Happy Valley permafrost soils, and a peak at wn 848 cm^{-1} was only present in Coastal Plain active-layer mineral-organic and mineral soils. In addition, all Coastal Plain horizons had a peak at wn 2516 cm^{-1} that was absent in the spectra of other soils, and all Sagwon Hills upland

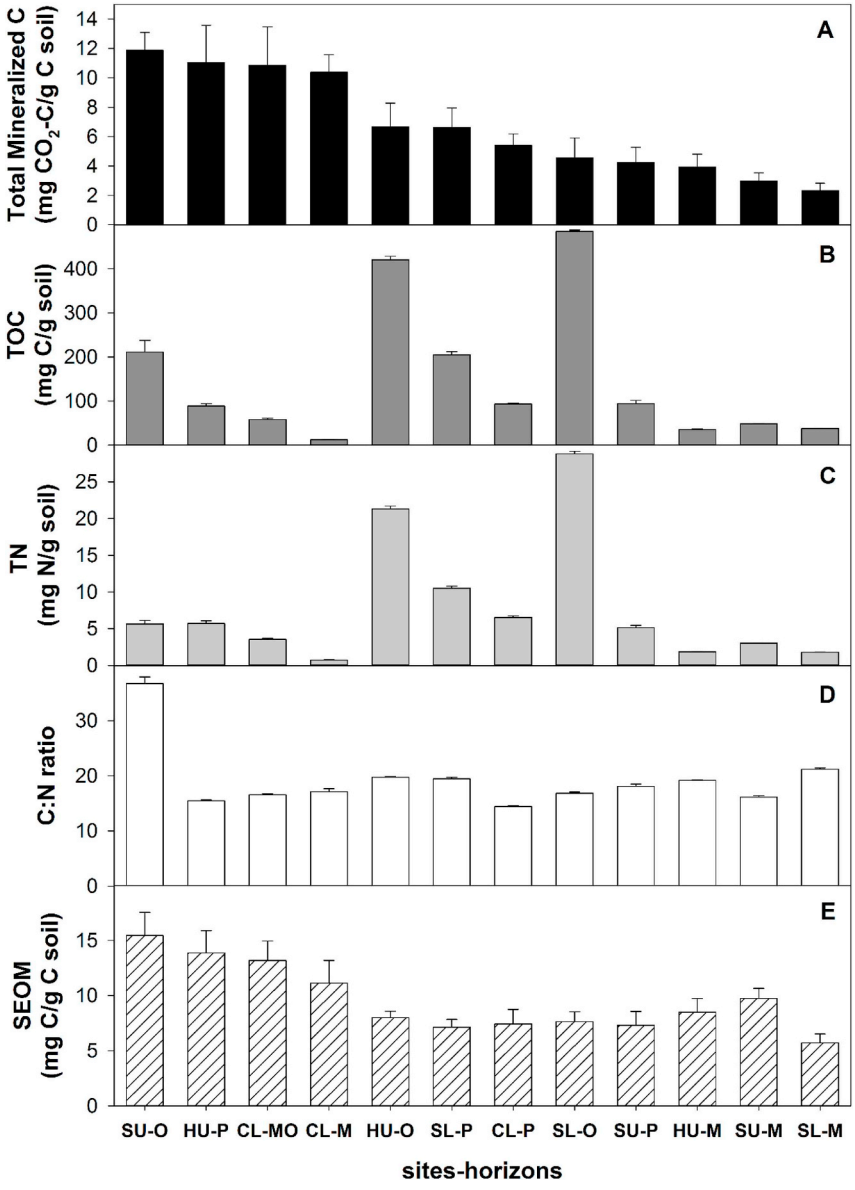

Fig. 2. Range of total mineralized C (A), TOC (B), TN (C), and C:N ratios (D) represented by the average of all incubated samples from each soil horizon at each site (O = active-layer organic, MO = active-layer organic-mineral, M = active-layer mineral, and P = mixed organic/mineral upper permafrost horizons; n = 20 for each horizon). Range of initial SEOM-C (E) is based on the average of 13 un-incubated samples from each soil horizon at each site.

horizons had a peak at wn 3694 cm^{-1}, which was missing from the spectra of all other soils except Sagwon Hills lowland mineral and permafrost horizons (Table 2). Other peaks, such as at wn 1270 and 1060 cm^{-1} were only found in organic horizon soils with the exception of Coastal Plain active-layer mineral-organic horizons. Similarly, a peak at wn 1788 cm^{-1} was present only in mineral soil spectra, with the exception of the Coastal Plain site where it occurred in all horizons (Table 2).

The capability of MIR spectra to predict soil TOC and TN concentrations and C:N ratios was excellent, while the prediction of 60-day mineralized C was good, when using all soils. The PLSR models for TOC, TN, and C:N produced very good correlations between the measured chemical data and the MIR predicted values (Fig. 5A, B, C). One spectral outlier, identified by the Mahalanobis Distance analysis, was removed from the calibration dataset for the TOC and TN calibration models (n = 239 spectra). The PLSR model for soil TOC concentration required 12 factors with R^2 = 0.9977, RMSE = 0.0737, and RPIQ = 26.7 (Fig. 5A). The PLSR model for soil TN concentrations required 17 factors with R^2 = 0.9960, RMSE = 0.0067, and RPIQ = 18.2 (Fig. 5B). The PLSR model for C:N ratios required 13 factors with R^2 = 0.9107, RMSE = 0.0320, and RPIQ = 2.4 (Fig. 5C). For predicting 60-day mineralized C, the Mahalanobis Distance analysis detected a total of eight concentration and spectral outliers that were removed from the PLSR calibration dataset (n = 232 spectra). The PLSR model for 60-day mineralized C required 9 factors with R^2 = 0.6542, RMSE = 0.2323, and an RPIQ = 2.4 (Fig. 5D). The capability of the PLSR model to predict mineralized C improved progressively for shorter incubation times. Indeed, compared to the PLSR model for 60-day mineralized C, R^2 and RPIQ for the 7-day mineralized C model increased by 9% and 17%, respectively, and RMSE was reduced by 73% (Table S1 supplemental material).

The factor 1 loadings for each of the PLSR models are shown in Fig. 6. Factor 1 loadings for TOC and TN overlapped and were indistinguishable from each other (Fig. 6). Overall, 11 peaks were identified for the TOC, TN, and C:N ratio loadings, denoting that a small number of wn were important for constructing the PLSR models. Loadings peak magnitudes for the other PLSR factors (2–10 for TOC and 2–13 for TN) varied, but the wn peaks were the same as those identified in the factor

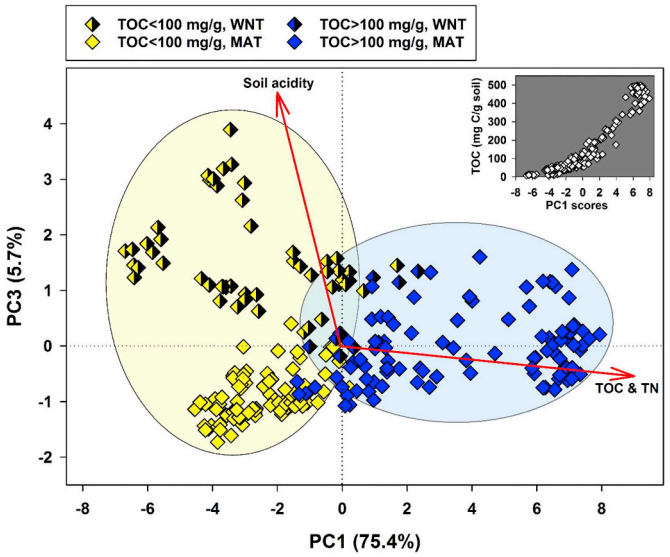

Fig. 3. Principal component analysis of the spectral data versus site and horizon characteristics. Diamonds indicate PCA scores (scores corresponding to soils with < 100 mg TOC/g soil are shown in yellow; scores corresponding to soils with > 100 mg TOC/g soil are shown in blue; full color scores correspond to acidic tundra sites; half black scores correspond to non-acidic tundra), ovals indicate sample grouping by PC1 and colors indicate the same designations as above, and red lines indicate significant correlation vectors. Figure insert shows PC1 scores versus soil TOC concentrations. (For interpretation of the references to color in this figure legend, the reader is referred to the Web version of this article.)

1 loadings (data not shown). Factor 1 loadings for the mineralized C model were almost a mirror image of those for TOC, TN, and C:N ratio, and the peaks were mostly all negative (Fig. 6). Loading factors 2 to 9 for the mineralized C model newly identified peaks at wn 3694, 2516, 1340, 874, and 811 cm^{-1} that were not found in the other models.

We explored whether PLSR models for predicting short-term mineralized C could be improved by splitting the soils into the groups defined by the influential factors and thresholds identified in the PCA. The best predictive model, and an improvement over the model produced using the entire dataset, was found for soils with low TOC and TN (Table 3). In contrast, PLSR predictive capability was reduced for soils with high TOC and TN. Grouping by tundra type also improved the PLSR model but only for acidic tundra (Table 3). The relationships between measured and predicted short-term mineralized C for the high TOC and low TOC models are compared in Fig. 7A. The β coefficients contributing to the low TOC model showed peaks at wn 3694–3620, 2924, 2852, 2516, 1788, 1634, 1528, 1473, 1380–1270, 874, 811, and 714 cm^{-1} (Fig. 7B), and the same peaks were observed for the low TN model. The peaks for the high TOC and TN models appeared to occur at the same wn, but their magnitude was greatly attenuated compared to the peaks for the low TOC and TN models, and some of the peaks, such as at wn 3694–3620, 2516, 1380-1270 disappeared (Fig. 7C).

4. Discussion

Our results indicate that MIR spectroscopy demonstrated the capability of predicting the concentration of TOC and TN of tundra soils and could also predict the short-term decomposability of these soils. MIR was particularly effective at determining the short-term decomposability for the active-layer mineral and upper permafrost soil horizons and/or soils with TOC concentrations of 100 mg C/g soil (10%) or lower. These findings suggest that MIR spectroscopy is a potential tool for quickly and reasonably estimating soil chemical properties and the short-term decomposability of the SOM stored in tundra soils.

Soil organic matter turnover and stability are largely controlled by environmental and biological factors (Schmidt et al., 2011), although the chemistry of SOM can also be an important factor influencing decomposition and soil respiration (Pisani et al., 2014). Across all incubations in this study, mineralized C varied among both sites and horizon types, but we only observed significantly greater mineralization for soils incubated at the highest temperature (16 °C). Even at 8 °C, mineralized C was not consistently greater than at 4° and 1 °C, and did not differ significantly (Fig. 1). Nadelhoffer et al. (1991) also found no difference in the mineralization rates of arctic soils incubated for 90 days between 3 °C and 9 °C, whereas greater rates occurred when the soils were incubated between 9 °C and 15 °C. The thawing of arctic soils has been shown to affect microbial community structure and soil metabolism (e.g., Coolen et al., 2011), with potential effects on SOM mineralization rates (Ernakovich et al., 2017). While these studies suggest that changes following thaw can be rapid (on the order of days to weeks), this response likely differs depending on soil conditions, temperature regime, and other factors, necessitating more research to understand when and how microbial community changes occur and their impacts. Nevertheless, in our short-term incubations, a change in microbial community structure and activity is a possible explanation for why 60-day C mineralization differed only at the highest incubation temperature. Indeed, at the end of our experiment, only soils incubated at 16 °C showed visual development of fungi covering the soil, suggesting a potential threshold for some microbial functional groups could have contributed to the substantial difference in SOM mineralization at this temperature.

As seen in other studies, readily bioavailable organic compounds are often the initial and major contributors to soil respiration in the short-term (Dutta et al., 2006; Neff and Hooper, 2002; Wu et al., 2014; Xu et al., 2009; Szymański, 2017). Indeed, we did observe a good correlation between mineralized C and the amount of SEOM in the soil (Fig. S1 Supplemental Material). Large amounts of readily decomposable C are usually present in the active layer from root exudates and plant litter, and the presence of wn peaks at 1656, 1270, and 1060 cm^{-1} in most of the organic layer soils, corresponding to polypeptides, phenolic OH, and carbohydrates respectively, appears to support this view in our soils (Fig. 4, Table 2). We also found a considerable amount of SEOM in mineral and upper permafrost soils (Fig. 2E), although they were lacking the most labile compounds found in the organic layer. Permafrost soils can contain and/or produce considerable amounts of labile C compounds as has been indicated by sustained soil respiration rates in some long-term studies (De Baets et al., 2016). This might likely be responding to the presence and amount of cryoturbated OM mixed in the permafrost layer, and due to the introduction of fresher OM materials at depth by frost churning processes (Ping et al., 2015).

The chemical composition of the soils, as shown by the MIR spectra, is typical of tundra and peaty/organic soils and is dominated by organic functional groups (e.g. Artz et al., 2008; Ernakovich et al., 2015; Matamala et al., 2017). Half of the identified absorbance bands were found in almost all soils, and most soils had peaks at wn 3622, 3394, 2924, 2852, 1993, 1870, 1616, 1521, 1423, 1380, 1159, 1000, and 811 cm^{-1}. Despite this uniformity, we found clear differences between tundra types that separated acidic from non-acidic tundra sites. All Coastal Plain soils consistently had high absorbance intensity at 2516 cm^{-1} wn, which has been shown to indicate the presence of carbonates and/or carboxylic acids in the soil (Parikh et al., 2014). In addition, the Coastal Plain site showed two distinct peaks at 873 and 848 cm^{-1} that were mostly unique to this site and might be also related to carbonates such as out of plane deformation CO_3 as shown by Tatzber et al. (2007), although they could also correspond to primary amine compounds (Smidt and Meissl, 2007). These differences most likely reflect the influence of underlying carbonate-rich loess blown in from the Sagavanirktok river floodplain in this location (Walker and Everett, 1991; Michaelson et al., 2012).

Most of the bands identified in this study were similarly found in tundra soils collected near the Sagwon Hills area and analyzed using

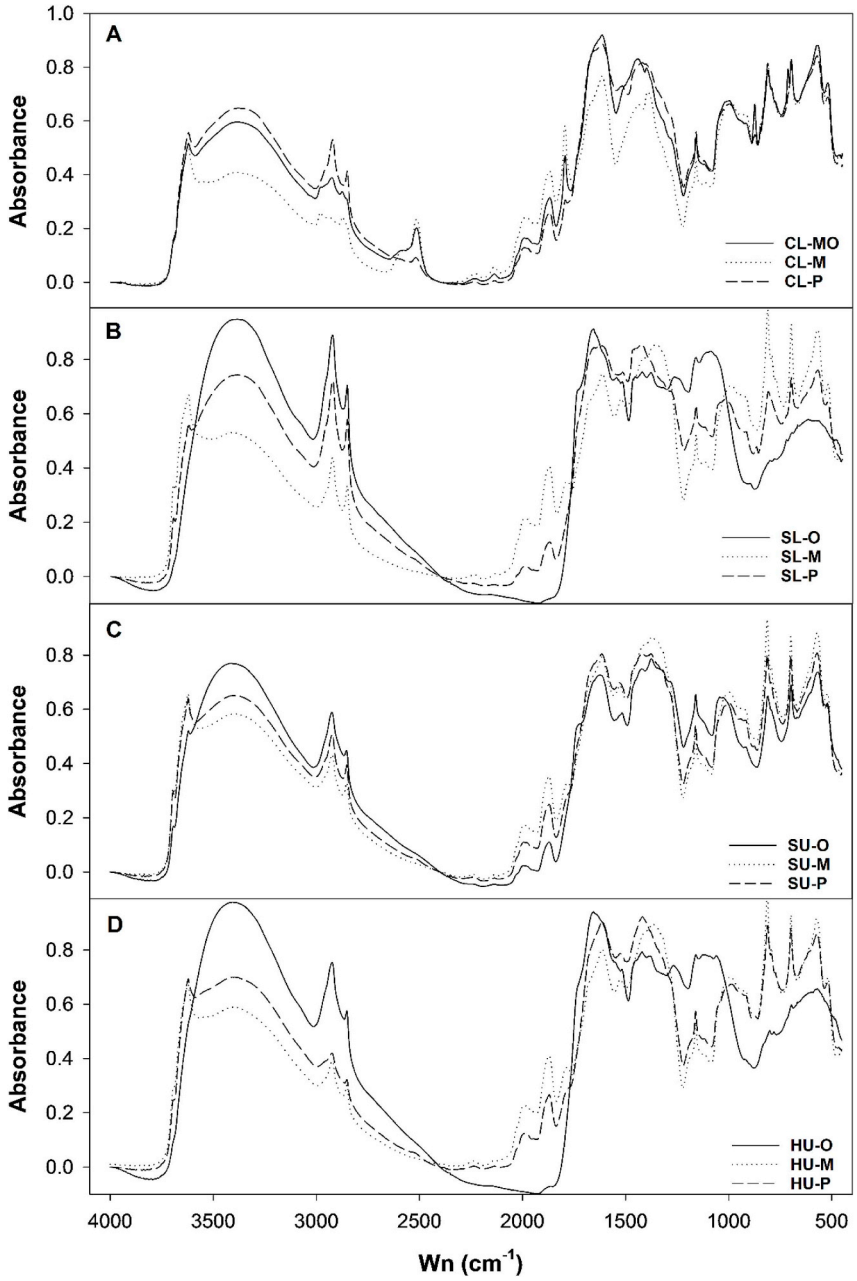

Fig. 4. Spectral means of active-layer organic (O), active-layer organic-mineral (MO), active-layer mineral (M), and mixed organic/mineral upper permafrost (P) horizons at each tundra site.

MIR by Ernakovich et al. (2015). These authors found the chemistries of SOM in the active-layer organic horizon and upper permafrost layer were more similar than that of the active-layer mineral horizon and suggested that cryoturbation of surface organic materials into the permafrost were responsible for those similarities. In our study, although it varied by site, we also found greater absorbance intensities for some of the organic functional bands in the organic active layer and the upper permafrost soils in comparison to the active-layer mineral soils. For example, greater band intensities for OH/NH at 3394 cm^{-1}, aliphatics at 2924 and 2852 cm^{-1}, aromatics or amine at 1656-1616 cm^{-1}, and carboxylic structures at 1423 cm^{-1}, indicated larger amounts of organic material in the upper permafrost compared to the mineral active layer. The mineral signatures of the mineral active layer and the upper permafrost soils were comparable at the Sagwon Hills lowland and upland, and Happy Valley sites, showing greater absorbance by clay minerals at 3622 and 1000 cm^{-1}, and quartz across the 1993-1788 cm^{-1} range and at 811 cm^{-1} than the organic soils at those sites. The mineral-organic and mineral active layer and upper permafrost soils were more uniform at the Coastal Plain site, likely an effect of deposition of river silts over the organic layer soils that have occurred for millennia (Ping et al., 1998; Michaelson et al., 2008).

Predictive models of soil properties have been constructed from MIR spectra across multiple-scales – from single sites to regions – and for many different soil types, with varying levels of accuracy (e.g., Janik et al., 1998; McBratney et al., 2006; Stenberg and Viscarra Rossel, 2010; Viscarra Rossel et al., 2006). Most models have used multivariate techniques, especially PLSR, to calibrate the infrared spectra of soils to various soil properties or other biogeochemical attributes. Yet, in some instances, predictions based on a specific wn or region of the spectrum can yield remarkably good results. Across a latitudinal gradient of Alaska soils representing a variety of grassland, forest and tundra systems, Matamala et al. (2017) found that a power regression function of

Table 2
Absorption bands and functional group assignment/s based on literature studies. Shaded areas indicate the peaks identified in Fig. 3 at each tundra site and horizon.

Wavenumber (cm^{-1})	Functional group	CL			SL			SU			HU		
		MO	M	P	O	M	P	O	M	P	O	M	P
3694	Clay minerals[a-e]					■	■	■	■	■			
3622	Clay minerals[a-e]	■	■	■		■	■	■	■	■		■	■
3394	O-H, H- bonded water, cellulose[f, g]	■	■	■	■	■	■	■	■	■	■	■	■
2984/2924	Aliphatic methyl & methylene groups[h-v]	■	■	■	■	■	■	■	■	■	■	■	■
2877/2852	Aliphatic methyl & methylene groups[h-v]	■	■	■	■	■	■	■	■	■	■	■	■
2516	Carbonates[h,m,q,x]	■	■	■									
2237	CN iso-cyanate, nitrile and cyanamide groups[w]	■	■	■		■				■		■	■
2137	Carbohydrates[p]	■	■	■									
1993	Silicates[a,z]	■	■	■		■	■	■	■	■		■	■
1870	Silicates[a,z]	■	■	■		■	■	■	■	■		■	■
1788	Silicates[a,z]	■	■	■		■			■			■	
1656	C=O of amide[d,g,n,o,q]				■						■		
1616	Aromatics[y] or amine[d]	■	■	■		■	■	■	■	■		■	■
1521	Lignin[g,k,q]			■	■	■		■	■	■	■	■	■
1423	Carboxylate/carboxylic structures[g]	■	■	■	■	■	■	■		■	■		■
1380	Phenolic, lignin[g]	■	■	■	■	■		■	■	■	■	■	
1270	Phenolic OH[f]				■			■			■		
1159	Polysaccharides[k], nucleic acids, proteins[k,o]	■	■	■	■	■	■	■	■	■	■	■	■
1116	n/a[*]		■			■				■		■	
1060	Carbohydrates[d,k,p]				■			■			■		
1000	Clay minerals[q,u]	■	■	■		■	■	■	■	■		■	■
916	Kaolinite and smectite[b,c,d]		■			■		■		■			
873	Carbonates[q]	■	■	■									■
848	Primary amine[q]	■	■										
811	Quartz[e]	■	■	■		■	■	■	■	■	■	■	■

[a]Nguyen et al., 1991; [b]Madejová and Komadel, 2001; [c]Nayak and Singh, 2007; [d]Viscarra Rossel and Behrens, 2010; [e]Churchman et al., 2010; [f]Veum et al., 2014; [g]Artz et al., 2008; [h]Soriano-Disla et al., 2014; [i]Ellerbrock and Gerke, 2004; [j]Haberhauer and Gerzabek, 1999; [k]Calderón et al., 2013; [l]Pedersen et al., 2011; [m]Bernier et al., 2013; [n]Leifield, 2006; [o]Movasaghi et al., 2008; [p]Janik et al., 2007; [q]Smidt and Meissl, 2007; [r]Niemeyer et al., 1992; [s]D'Acqui et al., 1999; [t]Du and Zhou, 2011; [u]Madejová, 2003; [v]Coates, 2000; [w]Francioso et al., 2009, 2011; [x]Parikh et al., 2014; [y]Verchot et al., 2011; [z]Calderón et al., 2011; [*]not identified in the literature.

the spectral band at 2922 cm^{-1} could predict TOC concentration with $R^2 = 0.85$. Nevertheless, multivariate models usually produce more robust calibration models. Indeed, the use of the whole spectra in this study linearized the relationship between MIR and TOC and TN concentrations and improved predictions over the single band function of Matamala et al. (2017). Not surprisingly, however, the aliphatic band at 2922 cm^{-1}, was still one of the most important bands in our PLSR calibration models. Other bands that were positively correlated with TOC and TN concentrations included phenolic OH at 3390 cm^{-1}, aromatics, C=O stretching, carboxylic acid COOH groups, and phenols at 1735, 1664, and 1225 cm^{-1} respectively, proteinaceous compounds at 1551 cm^{-1}, aliphatics and alcohols at 1170 cm^{-1}, and polysaccharides at 1088 cm^{-1}, whereas quartz bands were negatively correlated. Similar bands, although without 1088 cm^{-1} and with greater influence by the bands associated with smectite and kaolin clays, were found by Viscarra Rossel (2006) to be important drivers in a PLSR model of TOC concentration for sandy clay loam Australian soils. The effectiveness of these MIR bands in predicting TOC and TN in soil appears to be rather universal, but the relative contributions of different bands and the presence of competing interferences can vary across different soil types, affecting predictive capabilities (Janik et al., 1998; Viscarra Rossel et al., 2006).

Similar bands, but with some additions, exerted significant influence on the PLSR model for mineralized C, clearly indicating that soil MIR spectra contain information useful for predicting the results of biological activity. However, compared to TOC and TN, the mineralized C model had lower R^2 and higher RMSE suggesting that other factors, which may confound the relationship, likely play a role in predicting the short-term mineralization of SOM. One strategy for constructing better calibration models is to implement sample classification criteria that split the calibration samples into specific categories or groups that better represent sample characteristics (Soriano-Disla et al., 2014). The PCA analysis identified TOC and TN concentration thresholds, as well as tundra type, as important factors that influenced the MIR spectra. Splitting the dataset into groups according to these factors improved the mineralized C calibration model for soils with low TOC and TN concentrations. But, the calibration model for high TOC and TN soils, mostly from active-layer organic horizons, had lower predictive capability. Overall, splitting the dataset by tundra type did not improve predictions.

Separating the soils was more effective at determining mineralized C for the active-layer mineral and upper permafrost soil horizons and/or soils with TOC concentrations of 100 mg C/g soil or lower than the highly organic soils. It is possible that the large SOM background of the high TOC soils have masked the variations among the relevant wn predictors, affecting the predictive capability of the MIR spectra. This could be supported by the attenuation of the magnitude of the β coefficients' observed in the high TOC PLSR model. In addition, the quality of chemometric predictions can vary widely due to issues of sample size and different soil types (Viscarra Rossel et al., 2006). The active layer

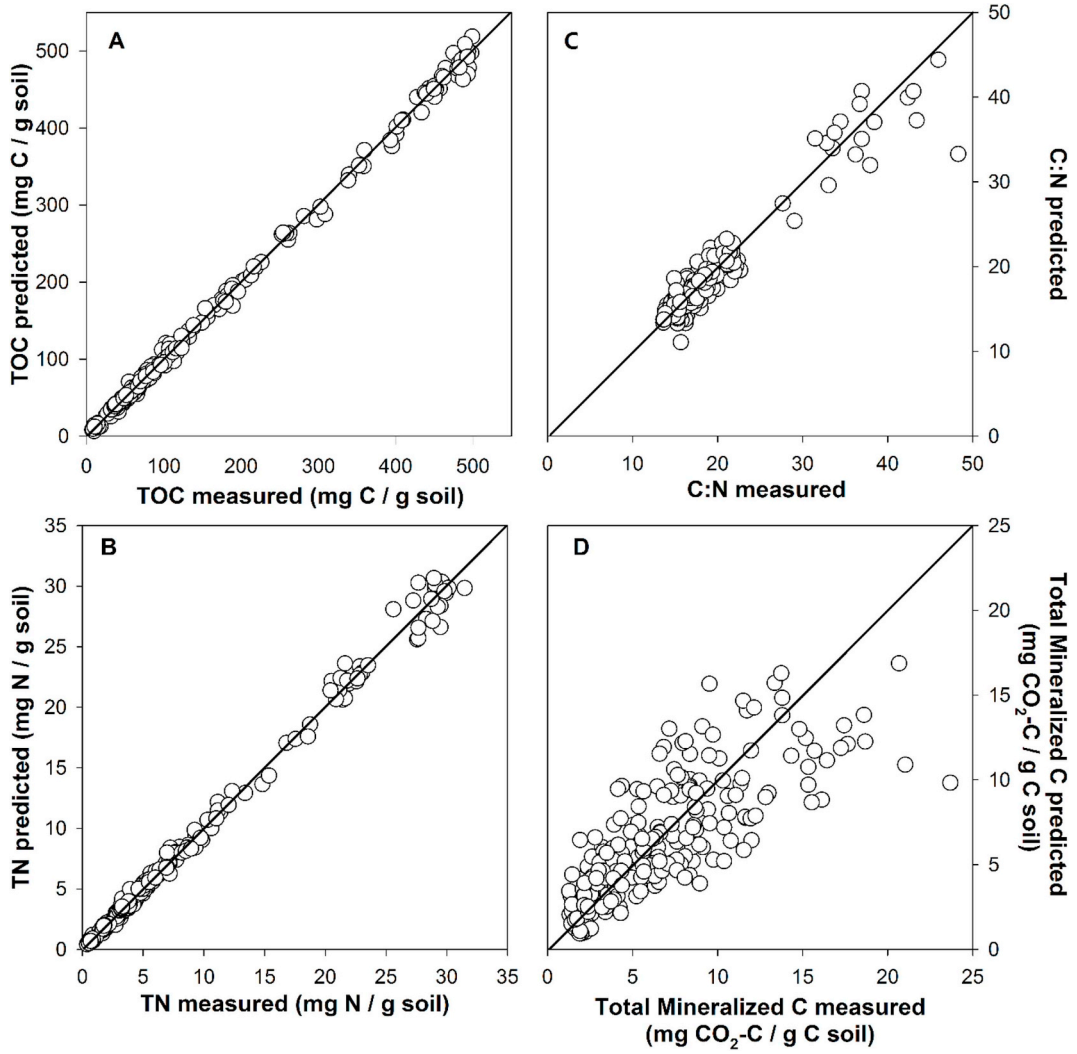

Fig. 5. Measured versus predicted soil TOC (A) and TN (B) concentrations, soil C:N ratios (C) and total mineralized C (D) derived from partial least square regression based on all acquired spectra.

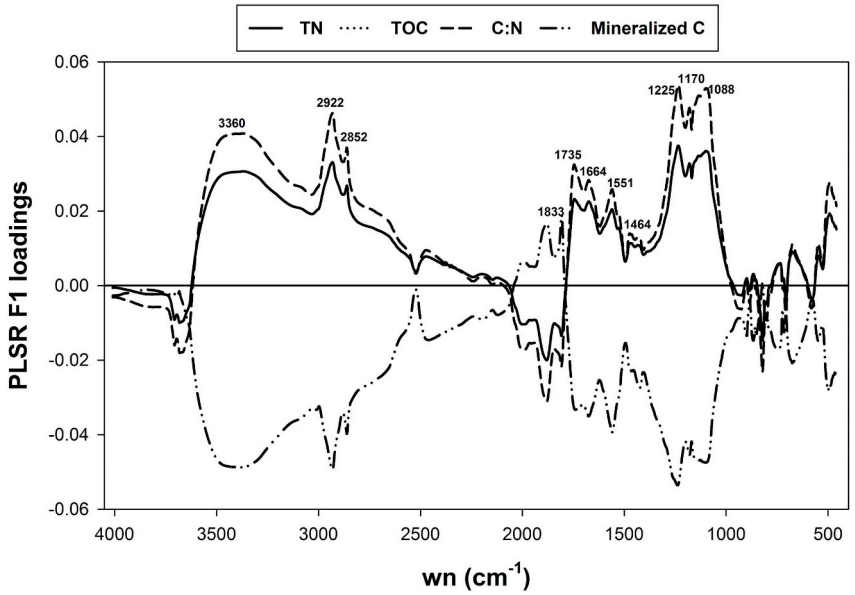

Fig. 6. Factor 1 loadings for partial least square regression models for soil TOC and TN concentrations, soil C:N ratios, and total mineralized C based on all acquired spectra.

Table 3
Sixty-day mineralized C model calibration statistics provided separately by TOC and TN concentrations and tundra type categories identified in the PCA analysis.

Category	n	# factors	R^2	RMSE	RPIQ
By TOC (%)					
TOC < 10%	131	12	0.7769	0.1843	3.3
TOC > 10%	96	6	0.5185	0.2365	2.1
By TN (%)					
TN < 0.6%	145	14	0.7637	0.1930	3.3
TN > 0.6%	85	6	0.4732	0.2390	1.9
By Tundra Type					
Acidic	177	6	0.6420	0.2370	2.7
Non-acidic	58	3	0.4982	0.2271	1.8

organic soils have a high variability in spectral properties due to differences in vegetation cover and to differences in the state of decomposition of the organic matter (Matamala et al., 2017). Because of this inherent heterogeneity, developing predictive PLSR models for mineralization of low decomposed, high organic soils might be especially challenging, needing larger calibration sets and perhaps the use of mathematical pretreatments of the spectral data. Similarly, because of the limited number of soils from non-acidic tundra compared to acidic tundra in our study, further investigations with a greater number of sites and soils representing these two tundra types will be required to determine the effect of acidity in the calibration models.

In the low TOC model, the wn relevant to predicting mineralized C were a mix of organic functional groups and mineral signatures with the amount of phenolic OH substrates exerting the greatest control over MIR predictions. The β coefficients revealed that mineralized C was positively correlated with the amount of carbonates, silicates, and C═O of amides in the soil. Mineralized C was negatively correlated with clays, aliphatic methyl and methylene groups, lignin, and phenolics content, which have been shown to increase with humification in some soils (Baldock et al., 1997; Kögel-Knabner, 1997). In Peltre et al. (2014), the CO_2 production in the 238-day soil incubations was also negatively correlated with aliphatic and aromatic wn and positively correlated with the carbonate and amide wn. In that study, a polysaccharide wn at 1100 was also positively correlated with the CO_2 production of the soils. Sugar amendments have enhanced the CO_2 production of soils in many incubation studies (e.g. Yang et al., 2016). In our incubations, the polysaccharides and the carbohydrate wn were important determinants only for the mineralization model when using the whole database, but the influence of these wn disappeared when mineralized C was predicted separately for the high and the low TOC soils. Overall, these results suggest that the capability of MIR to predict short-term mineralized C from tundra soils is mostly related to the association of SOM with the mineral clay fraction, and the amount of phenolic substrates present in the soil. Recent evidence that mineral-organic associations are relevant in determining SOM decomposability of permafrost soils was found by Gentsch et al. (2018) when the amount of mineralized C of permafrost soils at depth was not related to substrate quality but rather to mineral protection mechanisms that attenuated the effects of temperature sensibility of the SOM at depth. Therefore, physicochemical mechanisms in the soil environment, particularly, mineral protection of SOM, might underlay the relationship between the MIR spectra and the potential decomposability in these soils. Long-term incubations under different environmental conditions are needed to better understand this relationship.

5. Conclusions

In this study, PLSR models, constructed from MIR spectra, were excellent predictors of tundra soil TOC and TN concentrations. The PLSR model for predicting mineralized C in short-term incubations derived from all soils was good, but the best models were found for soils with lower TOC and TN concentrations. We suggest that MIR has the potential for quickly and reasonably estimating the short-term decomposability of tundra soils, particularly for soils from mineral horizons and organic enriched mineral soils with TOC concentrations < 10%. Analysis of the PLSR loadings and beta coefficients from the short-term decomposability models indicated a small number of influential spectral wn. These wn were associated with clay contents, phenolics, aliphatics, silicates, carboxylic acids, and amides. Additional incubations, focusing on changes (losses or additions) or relative differences between these influential organic functional groups and mineral components from across a wider geographic range, will be needed to determine the underlying factors controlling SOM mineralization rates and improve projections of carbon release from tundra soils. MIR predictive models calibrated from such studies coupled with widespread application of MIR measurements to already collected and archived arctic tundra soils could provide spatially referenced assessments of potential SOM decomposability across the region. Development of such a wide-ranging database could constrain and benchmark large-scale models simulating the mineralization rates of arctic tundra soils.

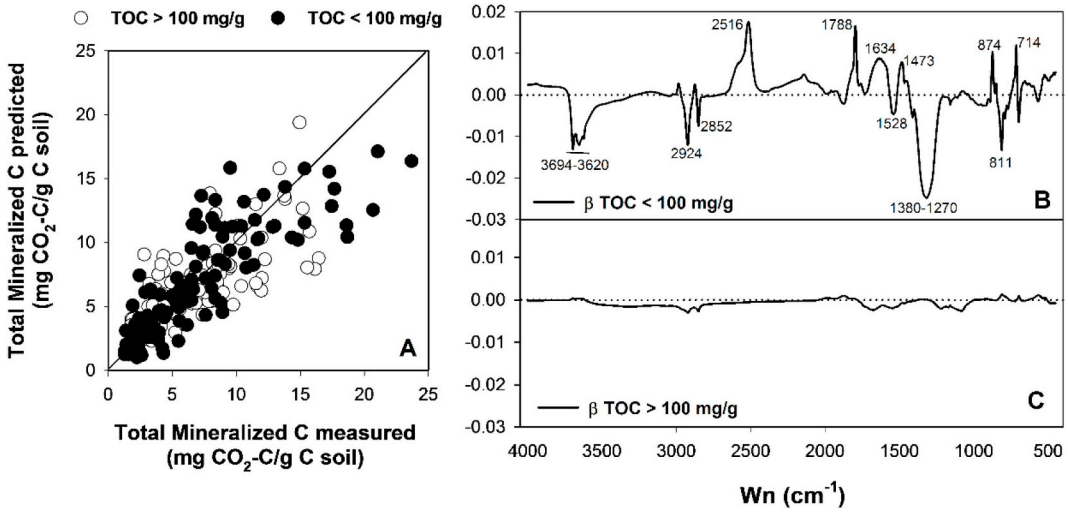

Fig. 7. Measured versus predicted total mineralized C (A) derived from partial least square regression models for soils with low and high TOC concentrations. Factor 1 β coefficients for partial least square regression models derived from low (B) and high (C) TOC soils. The threshold for separating low and high TOC soils = 100 mg C/g soil. Only the TOC models are shown, but the TN models showed the same at a threshold = 6 mg N/g soil.

Declaration of interest

None.

Acknowledgements

This work was supported by the United States Department of Energy, Office of Science, Office of Biological and Environmental Research under contract DE-AC02-06CH11357. G.J. Michaelson and C.L. Ping were also supported by the USDA-NIFA program. F. Calderón was supported by the United States Department of Agriculture, Agricultural Research Service. The use of trade, firm, or corporation names is for the information and convenience of the reader. Such use does not constitute an official endorsement or approval by the USDA or the Agricultural Research Service of any product or service to the exclusion of others that may be suitable. The USDA prohibits discrimination in all its programs and activities on the basis of race, color, national origin, age, disability, and where applicable, sex, marital status, familial status, parental status, religion, sexual orientation, genetic information, political beliefs, reprisal, or because all or part of an individual's income is derived from any public assistance program. We would like to thank S. Hofmann, J. Lederhouse, and T. Vugteveen for technical support and T. Patton for editorial work. The authors state no competing interests.

Appendix A. Supplementary data

Supplementary data related to this article can be found at https://doi.org/10.1016/j.soilbio.2018.10.014.

References

Artz, R.R.E., Chapman, S.J., Robertson, A.H.J., Potts, J.M., Laggoun-Défarge, F., Gogo, S., Comont, L., Disnar, J.-R., Francez, A.-J., 2008. FTIR spectroscopy can be used as a screening tool for organic matter quality in regenerating cutover peatlands. Soil Biology and Biochemistry 40, 515–527.

Baldock, J.A., Oades, J.M., Nelson, P.N., Skene, T.M., Golchin, A., Clarke, P., 1997. Assessing the extent of decomposition of natural organic materials using solid-state ^{13}C NMR spectroscopy. Australian Journal of Soil Research 35, 1035–1083.

Bellon-Maurel, V., Fernances-Ahumada, E., Palagos, B., Roger, J.M., McBratney, A., 2010. Critical review of chemometric indicators commonly used for assessing the quality of the prediction of soil attributes by NIR spectroscopy. Trends in Analytical Chemistry 29, 1073–1081.

Bernier, M.-H., Levy, G.J., Fine, P., Borisover, M., 2013. Organic matter composition in soils irrigated with treated wastewater: FTIR spectroscopy analysis of bulk soil samples. Geoderma 209, 233–240.

Bruun, S., Stenberg, B., Breland, T.A., Gudmundsson, J., Henriksen, T.M., Jensen, L.S., Korsæth, A., Luxhøia, J., Pálmasond, F., Pedersena, A., Salo, T., 2005. Empirical predictions of plant material C and N mineralization patterns from near infrared spectroscopy, stepwise chemical digestion and C/N ratios. Soil Biology and Biochemistry 3, 2283–2296.

Calderón, F.J., Reeves III, J.B., Collins, H.P., Paul, E.A., 2011. Chemical differences in soil organic matter fractions determined by diffuse-reflectance mid-infrared spectroscopy. Soil Science Society of America Journal 75, 568–579.

Calderón, F.J., Culman, S., Six, J., Franzluebbers, A.J., Schipanski, M., Beniston, J., Grandy, S., Kong, A.Y.Y., 2017. Quantification of soil permanganate oxidizable C (POXC) using infrared spectroscopy. Soil Science Society of America Journal 81, 277–288.

Chantigny, M.H., Angers, D.A., Kaiser, K., Kalbitz, K., 2008. Extraction and characterization of dissolved organic matter. In: Carter, M.R., Gregorich, E.G. (Eds.), Soil Sampling and Methods of Analysis, second ed. CRC Press, pp. 617–635.

Churchman, G.J., Foster, R.C., D'Acqui, L.P., Janik, L.J., SSkjemstad, J.O., Merry, R.H., Weissmann, D.A., 2010. Effect of land-use history on the potential for carbon sequestration in an Alfisol. Soil and Tillage Research 109, 23–35.

Coates, J., 2000. Interpretation of infrared spectra, a practical approach. In: Meyers, R.A. (Ed.), Encyclopedia of Analytical Chemistry. John Wiley & Sons, pp. 10815–10837.

Coolen, M.J.L., VanDeGiessen, J., Zhu, E.Y., Wuchter, C., 2011. Bioavailability of soil organic matter and microbial community dynamics upon permafrost thaw. Environmental Microbiology 13, 2299–2314.

D'Acqui, L.P., Churchman, G.J., Janik, L.J., Ristori, G.G., Weissmann, D.A., 1999. Effect of organic matter removal by low-temperature ashing on dispersion of undisturbed aggregates from a tropical crusting soil. Geoderma 93, 311–324.

De Baets, S., van de Weg, M.J., Lewis, R., Steinberg, N., Meersmans, J., Quine, T.A., Shaver, G.R., Hartley, I.P., 2016. Investigating the controls on soil organic matter decomposition in tussock tundra soil and permafrost after fire. Soil Biology and Biochemistry 99, 108–116.

Du, C.W., Zhou, J.M., 2011. Application of infrared photoacoustic spectroscopy in soil analysis. Applied Spectroscopy Reviews 46, 405–422.

Duboc, O., Tintner, J., Zehetner, F., Smidt, E., 2016. Does sample drying temperature affect the molecular characteristics of organic matter in soils and litter? A statistical proof using ATR infrared spectra. Vibrational Spectroscopy 85, 215–221.

Duckworth, J.H., 1998. Spectroscopic quantitative analysis. In: Workman Jr.J., Springsteen, A. (Eds.), Applied Spectroscopy. A Compact Reference for Practitioners. Academic Press, pp. 93–159.

Dutta, K., Schuur, E.A.G., Neff, J.C., Zimov, S.A., 2006. Potential carbon release from permafrost soils of Northeastern Siberia. Global Change Biology 12, 2336–2351.

Elberling, B., Michelsen, A., Schädel, C., Schuur, E.A.G., Christiansen, H.H., Berg, L., Tamstorf, M.P., Sigsgaard, C., 2013. Long-term CO_2 production following permafrost thaw. Nature Climate Change 3, 890–894.

Ellerbrock, R.H., Gerke, H.H., 2004. Characterizing organic matter of soil aggregate coatings and biopores by Fourier transform infrared spectroscopy. European Journal of Soil Science 55, 219–228.

Ernakovich, J.G., Wallenstein, M.D., Calderón, F.J., 2015. Chemical indicators of cryoturbation and microbial processing throughout an Alaskan permafrost soil. Soil Science Society of America Journal 79, 783–793.

Ernakovich, J.G., Lynch, L.M., Brewer, P.E., Calderón, F.J., Wallenstein, M.D., 2017. Redox and temperature-sensitive changes in microbial communities and soil chemistry dictate greenhouse gas loss from thawed permafrost. Biogeochemistry 134, 183–200.

Fierer, N., Colman, B.P., Schimel, J.P., Jackson, R.B., 2006. Predicting the temperature dependence of microbial respiration in soil: a continental-scale analysis. Global Biogeochemical Cycles 20, GB3026. https://doi.org/10.1029/2005GB002644.

Gentsch, N., Wild, B., Mikutta, R., Capek, P., Diáková, K., Schrumpf, M., Turner, S., Minnich, C., Schaarschmidt, F., Shibistova, O., Schnecker, J., Urich, T., Gittel, A., Santrucková, H., Bárta, J., Lashchinskiy, N., FuB, R., Richter, A., Guggenberger, G., 2018. Temperature response of permafrost soil carbon is attenuated by mineral protection. Global Change Biology 24, 3401–3415.

Gillespie, A.W., Sanei, H., Diochon, A., Ellert, B.H., Regier, T.Z., Chevrier, D., Dynes, J.J., Tarnocai, C., Gregorich, E.G., 2014. Perennially and annually frozen soil carbon differ in their susceptibility to decomposition: analysis of Subarctic earth hummocks by bioassay, XANES and pyrolysis. Soil Biology and Biochemistry 68, 106–116.

Haberhauer, G., Gerzabek, M.H., 1999. DRIFT and transmission FT-IR spectroscopy of forest soils: an approach to determine decomposition processes of forest litter. Vibrational Spectroscopy 19, 413–417.

Janik, L.J., Merry, R.H., Skjemstad, J.O., 1998. Can mid infrared diffuse reflectance analysis replace soil extractions? Australian Journal of Experimental Agriculture 38, 681–696.

Janik, L.J., Skjemstad, J.O., Shepherd, K.D., Spouncer, L.R., 2007. The prediction of soil carbon fractions using mid-infrared-partial least square analysis. Australian Journal of Soil Research 45, 73–81.

Knoblauch, C., Beer, C., Sosnin, A., Wagner, D., Pfeiffer, E.M., 2013. Predicting long-term carbon mineralization and trace gas production from thawing permafrost of Northeast Siberia. Global Change Biology 19, 1160–1172.

Kögel-Knabner, I., 1997. ^{13}C and ^{15}N NMR spectroscopy as a tool in soil organic matter studies. Geoderma 80, 243–270.

Lee, H., Schuur, E.A.G., Inglett, K.S., Lavoie, M., Chanton, J.P., 2012. The rate of permafrost carbon release under aerobic and anaerobic conditions and its potential effects on climate. Global Change Biology 18, 515–527.

Leifield, J., 2006. Application of diffuse reflectance FT-IR spectroscopy and partial least-squares regression to predict NMR properties of soil organic matter. European Journal of Soil Science 57, 846–857.

Leinweber, P., Jandl, G., Baum, C., Eckhardt, K.-U., Kandeler, E., 2008. Stability and composition of soil organic matter control respiration and soil enzyme activities. Soil Biology and Biochemistry 40, 1496–1505.

Madejová, J., 2003. FTIR techniques in clay mineral studies. Vibrational Spectroscopy 31, 1–10.

Madejová, J., Komadel, P., 2001. Baseline studies of the clay minerals society source clays: infrared methods. Clays and Clay Minerals 49 470–432.

Mann, B.F., Chen, H., Herndon, E.M., Chu, R.K., Tolic, N., Portier, E.F., Chowdhury, T.R., Robinson, E.W., Callister, S.J., Wullschleger, S.D., Graham, D.E., Liang, L., Gu, B., 2015. Indexing permafrost soil organic matter degradation using high-resolution mass spectrometry. PloS One 10, e0130557. https://doi.org/10.1371/journal.pone.0130557.

Matamala, R., Calderón, F.J., Jastrow, J.D., Fan, Z., Hofmann, S.M., Michaelson, G.J., Mishra, U., Ping, C.L., 2017. Influence of site and soil properties on the DRIFT spectra of northern cold-region soils. Geoderma 305, 80–91.

McBratney, A.B., Minasny, B., Rossel, R.V., 2006. Spectral soil analysis and inference systems: a powerful combination for solving the soil data crisis. Geoderma 136, 272–278.

Michaelson, G.J., Ping, C.L., 2003. Soil organic carbon and CO_2 respiration at subzero temperature in soils of Arctic Alaska. Journal of Geophysical Research 108, 8164.

Michaelson, G.J., Ping, C.L., 2017. Guidebook Alaska soil geography field study – permafrost-affected soils. Agriculture and Forestry Experimental Station Bulletin 118 (School of Natural Resources and Extension, University of Alaska Fairbanks).

Michaelson, G.J., Ping, C.L., Epstein, H., Kimble, J.M., Walker, D.A., 2008. Soils and frost boil ecosystems across the North american arctic transect. Journal of Geophysical Research-Biogeosciences 113, G3.

Michaelson, G.J., Ping, C.L., Walker, D.A., 2012. Soils associated with biotic activity on frost boils in Arctic Alaska. Soil Science Society of America Journal 76, 2265–2277.

Michaelson, G.J., Ping, C.L., Clark, M.H., 2013. Soil pedon carbon and nitrogen data for Alaska: an analysis and update. Open Journal of Soil Science 3, 132–142.

Movasaghi, Z., Rehman, S., Rehman, I.U., 2008. Fourier transform infrared (FTIR)

spectroscopy of biological tissues. Applied Spectroscopy Reviews 43, 134–179.
Nadelhoffer, K.J., Giblin, A.E., Shaver, G.R., Laundre, J.A., 1991. Effects of temperature and substrate quality on element mineralization in six arctic soils. Ecology 72, 242–253.
Nayak, P., Singh, B.K., 2007. Instrumental characterization of clay by XRF, XRD and FTIR. Bulletin of Materials Science 30, 235–238.
Neff, J.C., Hooper, D.U., 2002. Vegetation and climate controls on potential CO_2, DOC and DON production in northern latitude soils. Global Change Biology 8, 872–884.
Nguyen, T.T., Janik, L.J., Raupach, M., 1991. Diffuse reflectance infrared Fourier transform (DRIFT) spectroscopy in soil studies. Australian Journal of Soil Research 29, 49–67.
Niemeyer, J., Chen, Y., Bollag, J.M., 1992. Characterization of humic acids, composts, and peat by diffuse reflectance Fourier-transform infrared-spectroscopy. Soil Science Society of America Journal 56, 135–140.
Parikh, S.J., Goyne, K.W., Margenot, A.J., Mukome, F.N.D., Calderón, F.J., 2014. Soil chemical insights provided through vibrational spectroscopy. Advances in Agronomy 126, 1–148.
Pedersen, J.A., Simpson, M.A., Bockheim, J.G., Kumar, K., 2011. Characterization of soil organic carbon in drained thaw-lake basins of Arctic Alaska using NMR and FTIR photoacoustic spectroscopy. Organic Geochemistry 42, 947–954.
Peltre, P., Brunn, S., Du, C., Thomsen, I.K., Jensen, L.S., 2014. Assessing soil constituents and labile soil organic carbon by mid-infrared photoacoustic spectroscopy. Soil Biology and Biochemistry 77, 41–50.
Ping, C.L., Bockheim, J.G., Kimble, J.M., Michaelson, G.J., Walker, D.A., 1998. Characteristics of cryogenic soils along a latitudinal transect in Arctic Alaska. Journal of Geophysical Research-Atmospheres 103, 28917–28928.
Ping, C.L., Clark, M.H., Kimble, J.M., Michaelson, G.J., Shur, Y., Stiles, C.A., 2013. Sampling protocols for permafrost-affected soils. Soil Horizons 54, 13–19.
Ping, C.L., Jastrow, J.D., Michaelson, G.J., Jorgenson, M.T., Shur, Y.L., 2015. Permafrost soils and carbon cycling. SOIL 1, 147–171.
Pisani, O., Hills, K.M., Courtier-Murias, D., Haddix, M.L., Paul, E.A., Conant, R.T., Simpson, A.J., Arhonditsis, G.B., Simpson, M.J., 2014. Accumulation of aliphatic compounds in soil with increasing mean annual temperature. Organic Chemistry 76, 118–127.
Provin, T., 2014. Total carbon and nitrogen and organic carbon via thermal combustion analysis. In: Sikora, F.J., Moore, K.P. (Eds.), Soil Test Methods from the Southeastern United States. Southern Cooperative Series Bulletin No. 419, Southern Extension and Research Activity Information Exchange Group - 6, pp. 149–154. available online at: http://www.clemson.edu/sera6/MethodsManualFinalSERA6.pdf.
Schädel, C., Schuur, E.A.G., Bracho, R., Elberling, B., Knoblauch, C., Lee, H., Luo, Y., Shaver, G.R., Turetsky, M.R., 2014. Circumpolar assessment of permafrost C quality and its vulnerability over time using long-term incubation data. Global Change Biology 20, 641–652.
Schimel, J.P., Mikan, C., 2005. Changing microbial substrate use in Arctic tundra soils through a freeze-thaw cycle. Soil Biology and Biochemistry 37, 1411–1418.
Schmidt, M.W., Torn, M.S., Abiven, S., Dittmar, T., Guggenberger, G., Janssens, I.A., Kleber, M., Kogel-Knabner, I., Lehmann, J., Manning, D.A.C., Nannipieri, P., Rasse, D.P., Weiner, S., Trumbore, S.E., 2011. Persistence of soil organic matter as an ecosystem property. Nature 478, 49–55.
Schuur, E.A.G., McGuire, A.D., Schädel, C., Grosse, G., Harden, J.W., Hayes, D.J., Hugelius, G., Koven, C.D., Kuhry, P., Lawrence, D.M., Natali, S.M., 2015. Climate change and the permafrost carbon feedback. Nature 520 (7546), 171–179.
Shaver, G.R., Giblin, A.E., Nadelhoffer, K.J., Thieler, K.K., Downs, M.R., Laundre, J.A., Rastetter, E.B., 2006. Carbon turnover in Alaskan tundra soils: effects of organic matter quality, temperature, moisture and fertilizer. Journal of Ecology 94, 740–753.
Smidt, E., Meissl, K., 2007. The applicability of Fourier transform infrared (FT-IR) spectroscopy in waste management. Waste Management 27, 268–276.
Soong, J.L., Parton, W.J., Calderon, F., Campbell, E.E., Cotrufo, M.F., 2015. A new conceptual model on the fate and controls of fresh and pyrolized plant litter decomposition. Biogeochemistry 124, 27–44.
Soriano-Disla, J.M., Janik, L.J., Viscarra Rossel, R.A., Macdonald, L.M., McLaughlin, M.J., 2014. The performance of visible, near-, and mid-infrared reflectance spectroscopy for prediction of soil physical, chemical, and biological properties. Applied Spectroscopy Reviews 49, 139–186.
Stenberg, B., Viscarra Rossel, R.A., 2010. Diffuse reflectance spectroscopy for high-resolution soil sensing. In: Viscarra Rossel, R.A. (Ed.), Proximal Soil Sesing, Progress in Socil Science. Springer Science + Business Media, New York, pp. 29–47.
Stumpe, B., Weihermuller, L., Marschner, B., 2011. Sample preparation and selection for qualitative and quantitative analyses of soil organic carbon with mid-infrared reflectance spectroscopy. European Journal of Soil Science 62, 849–862.
Szymański, W., 2017. Quantity and chemistry of water-extractable organic matter in surface horizons of Arctic soils under different types of tundra vegetation – a case study from the Fuglebergsletta coastal plain (SW Spitsbergen). Geoderma 305, 30–39.
Tatzber, M., Stemmer, M., Spiegel, H., Katzlberger, C., Haberhauer, G., Gerzabek, M.H., 2007. An alternative method to measure carbonate in soils by FT-IR spectroscopy. Environmental Chemistry Letters 5, 9–12.
Thomsen, I.K., Bruun, S., Jensen, L.S., Christensen, B.T., 2009. Assessing soil carbon lability by near infrared spectroscopy and NaOCl oxidation. Soil Biology and Biochemistry 41, 2170–2177.
Tinti, A., Tugnoli, V., Bonora, S., Francioso, O., 2015. Recent applications of vibrational mid-Infrared (IR) spectroscopy for studying soil components: a review. Journal of Central European Agriculture 16, 1–22.
Uhlířová, E., Šantrůčková, H., Davidov, S.P., 2007. Quality and potential biodegradability of soil organic matter preserved in permafrost of Siberian tussock tundra. Soil Biology and Biochemistry 3, 1978–1989.
Verchot, L.V., Dutaur, L., Shepherd, K.D., Albrecht, A., 2011. Organic matter stabilization in soil aggregates: understading the biogeochemical mechanisms that determine the fate of carbon inputs in soils. Geoderma 161, 182–193.
Veum, K.S., Goyne, K.W., Kremer, R.J., Miles, R.J., Sudduth, K.A., 2014. Biological indicators of soil quality and soil organic matter characteristics in an agricultural management continuum. Biogeochemistry 117, 81–99.
Viscarra Rossel, R.A., Behrens, T., 2010. Using data mining to model and interpret soil diffuse reflectance spectra. Geoderma 158, 46–54.
Viscarra Rossel, R.A., Walvoort, D.J.J., McBratney, A.B., Janik, L.J., Skjemstad, J.O., 2006. Visible, near infrared, mid infrared or combined diffuse reflectance spectroscopy for simultaneous assessment of various soil properties. Geoderma 131, 59–75.
Waldrop, M.P., Wickland, K.P., White III, R., Berhe, A.A., Harden, J.W., Romanovsky, V.E., 2010. Molecular investigations into a globally important carbon pool: permafrost-protected carbon in Alaskan soils. Global Change Biology 16, 2543–2554.
Walker, D.A., Everett, K.R., 1991. Loess ecosystems of northern Alaska – regional gradient and toposequence at Prudhoe Bay. Ecological Monographs 61, 427–464.
Walker, D.A., Epstein, H.E., Gould, W.A., Kelley, A.M., Kade, A.N., Knudson, J.A., Krantz, W.B., Michaelson, G.J., Peterson, R.A., Ping, C.L., Raynolds, M.K., Romanovsky, V.E., Shur, Y., 2004. Frost-boil ecosystems: complex interactions between landforms, soils, vegetation, and climate. Permafrost Periglacial 15, 171–188.
Weintraub, M.N., Schimel, J.P., 2003. Interactions between carbon and nitrogen mineralization and soil organic matter chemistry in Arctic tundra soils. Ecosystems 6, 129–143.
Wild, B., Schnecker, J., Alves, R.J.E., Barsukov, P., Bárta, J., Čapek, P., Gentsch, N., Gittel, A., Guggenberger, G., Lashchinskiy, N., Mikutta, R., Rusalimova, O., Šantrůčková, H., Shibistova, O., Urich, T., Watzka, M., Zrazhevskaya, G., 2014. Input of easily available organic C and N stimulates microbial decomposition of soil organic matter in arctic permafrost soil. Soil Biology and Biochemistry 75, 143–151.
Wu, X.D., Fang, H.B., Zhao, L., Wu, T.H., Li, R., Ren, Z.W., Pang, Q.Q., Ding, Y.J., 2014. Mineralization and changes in the fractions of soil organic matter in soils of the permafrost regions, Qinghai-Tibet Plateau, China. Permafrost and Periglacial Processes 25, 35–44.
Xu, C., Guo, L., Ping, C.L., White, D.M., 2009. Chemical and isotopic characterization of size-fractionated organic matter from cryoturbated tundra soils, northern Alaska. Journal of Geophysical Research 114, G03002.
Yang, Z., Wullschleger, S.D., Liang, L., Graham, D.E., Gu, B., 2016. Effects of warming on the degradation and production of low-molecular-weight labile organic carbon in an Arctic tundra soil. Soil Biology and Biochemistry 95, 202–211.